MODELLING THE TENSILE FAILURE OF HYBRID POLYMER COMPOSITES

Rodrigo P. Tavares[1,2], António R. Melro[3], Albert Turon[4], Pedro P. Camanho[1,2]

[1]DEMec, Faculdade de Engenharia, Universidade do Porto, Rua Dr. Roberto Frias, 4200-465 Porto, Portugal
[2]INEGI, Rua Dr. Roberto Frias, 400, 4200-465 Porto, Portugal
[3]Advanced Composites Centre for Science and Innovation (ACCIS), University of Bristol, Queens Building, University Walk, Bristol, UK
[4]AMADE, Polytechnic School, University of Girona, Campus Montilivi s/n, 17071 Girona, Spain

Keywords: Hybrid composites, Numerical modelling, Analytical modelling,

Abstract

In this work a micromechanical model that takes into account the statistical nature of fibre strength present in composite materials, as well as the proper constitutive response of the resin and fibre-matrix interface, is developed and used to determine the failure behaviour of hybrid and non-hybrid composite materials. The model is able to capture failure mechanisms in the three main components of a composite material: fibres, matrix and fibre-matrix interface. The understanding of the failure mechanisms is used to modify the tensile behaviour of hybrid composites to have a pseudo-ductile behaviour.

1. Introduction

Fibre-reinforced composites, play an important role in structural applications, however their use is partly hampered due to the low toughness they exhibit. Fibre hybridisation is a strategy that can lead to improved composite properties and performance, as it not only changes the material properties but also changes the damage propagation mechanisms leading to final failure [1, 2].

The objective of this work is to study the effects of fibre hybridization on the tensile failure of unidirectional hybrid composites. Taking into account that fibre-reinforced composites are complex materials with multiple constituents it is hard to assess the effects that each of the constituents properties have on the behaviour of composite materials, therefore, reliable models for the tensile failure of hybrid composites are essential.

Usually composite materials undergo catastrophic failure with a stress-strain diagram as presented in Figure 1a. Hybridizing the composite material changes the failure process which results in stress-strain diagrams similar to Figure 1b, where the two load drops correspond, respectively, to the failure of the LE fibres and the HE fibres. The objective of this work is to model the tensile failure of hybrid composites and to under- stand the mechanism and failure sequence in these materials. By understanding the controlling factors in the behaviour of hybrid composite materials it is possible to design a material with either an hybrid effect (Figure 1b) or with a pseudo-ductile behaviour (Figure 1c).

Excerpt from ISBN 978-3-00-053387-7

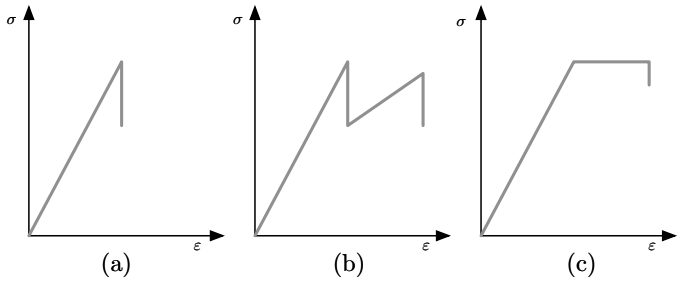

Figure 1. Schematic stress-strain diagrams for: (a) non-hybrid composites, (b) typical hybrid composites and (c) pseudo-ductile hybrid composites.

2. Numerical model

To accurately capture the failure mechanisms and to study their effects on the composite behaviour it is necessary to to resort to direct numerical simulation, namely micro-scale numerical models that are able to distinguish the behaviour of the various components and accurately represent the interaction between them [2]. In the micro-scale numerical models it is necessary to develop a Representative Volume Element (RVE) that is able to represent the material response. Several authors [3–5] have studied the development of clusters of broken fibres, which are the main mechanism that trigger failure of unidirectional composites loaded in the longitudinal direction. As this cluster development needs to be captured in the RVE and is usually considered to be composed of around 20 fibres, it was decided that the RVE would have in the fibre's transverse direction a length equal to 15 times the fibre radius. In the longitudinal direction it is necessary that the RVE captures the full extent of the ineffective length in a broken fibre. This lead to the choice of a longitudinal size for the RVE also equal to 15 times the fibre radius. The fibre generation in the RVE was done using a modified version of the random fibre generator developed by Melro et al. [6] to accurately represent the real microstructure of a composite material. The generated RVEs have approximately 3 million elements and are composed of Abaqus® C3D8R and C3D6R elements [7].

As there are different constituents in a composite material it is necessary to define different damage models for each that are able to accurately capture the response and failure of these materials.

2.1. Fibre model

The fibres are considered to be linear elastic up to failure and to have a transversely isotropic behaviour. The complementary free energy is defined as:

$$\begin{aligned}\mathscr{G}_f =& \frac{\sigma_{11}^2}{2E_1\left(1-d_f\right)} + \frac{\sigma_{22}^2+\sigma_{33}^2}{2E_2\left(1-d_f\right)} - \frac{\nu_{12}}{E_1}\left(\sigma_{11}\sigma_{22}+\sigma_{11}\sigma_{33}\right) - \frac{\nu_{23}}{E_2}\sigma_{22}\sigma_{33} \\ &+ \frac{\sigma_{12}^2+\sigma_{13}^2}{2G_{12}\left(1-d_f\right)} + \frac{\sigma_{23}^2}{2G_{23}\left(1-d_f\right)},\end{aligned} \tag{1}$$

where E_1 and E_2 are the longitudinal and transverse Young's moduli, G_{12} and G_{23} the longitudinal and transverse shear moduli and d_f is the damage variable for the fibres.

Excerpt from ISBN 978-3-00-053387-7

The compliance tensor ($\boldsymbol{H_f}$) can be defined as:

$$\boldsymbol{H_f} = \frac{\partial^2 \mathscr{G}_f}{\partial \boldsymbol{\sigma}^2} \ . \tag{2}$$

Inverting the compliance tensor results in the stiffness tensor ($\boldsymbol{C_f}$). The damage activation function can be defined as:

$$F_f^d = \phi_f^d - r_f \leq 0 \ , \tag{3}$$

where ϕ_f^d is the loading function

$$\phi_f^d = \frac{\tilde{\sigma}_{11}}{X_f^t} \ , \tag{4}$$

and r_f the internal variable

$$r_f = \max\left\{1, \max_{t\to\infty}\left\{\phi_{f,t}^d\right\}\right\} \ . \tag{5}$$

The loading function is function of the fibre tensile strength (X_f^t), which has a stochastic value and will vary from element to element. To avoid mesh dependency problems and to control the energy dissipated in the fracture process, Bažant's crack band model [8] was implemented. The dissipated energy for the fibres is defined as:

$$\Psi_f = \int_0^\infty Y_f \dot{d}_f \, \mathrm{d}t = \int_1^\infty \frac{\partial \mathscr{G}_f}{\partial d_f}\frac{\partial d_f}{\partial r_f} \, \mathrm{d}r_f = \frac{G_{ff}}{l^e} \ , \tag{6}$$

where G_{ff} is the fracture toughness of the fibres in mode I, l^e the element's characteristic length and Y_f is the thermodynamic force associated with the variable d_f. As the tensile strength of the fibres is a stochastic parameter a random strength is assigned to each element that represents the fibre. This is done by generating random numbers (X) in the range 0 to 1 and by using the Weibull distribution it is possible to calculate the random tensile strength:

$$X_f^t = \sigma_0 \left[-\frac{L_0}{L}\ln\left(1 - X\right)\right]^{1/m} \ . \tag{7}$$

2.2. Matrix model

The matrix is modelled using the model proposed by Melro et al. [9]. The matrix is considered to have a non-linear behaviour controlled by a paraboloidal yield criterion, being the yield surface defined as:

$$\Phi\left(\boldsymbol{\sigma}, \sigma_c, \sigma_t\right) = 6J_2 + 2I_1\left(\sigma_c - \sigma_t\right) - 2\sigma_c\sigma_t \ , \tag{8}$$

where σ_c and σ_t are, respectively, the compressive and tensile yield strengths of the matrix material, J_2 is the second invariant of the deviatoric tensor and I_1 the first invariant of the stress tensor. The model also considers isotropic damage for the matrix, using a single damage variable that affects the stiffness of the material. The damage model is similar to the one for the fibres, however the damage activation function and damage evolution law are given by:

$$\phi_m^d = \frac{3\tilde{J}_2}{X_m^c X_m^t} + \frac{\tilde{I}_1\left(X_m^c - X_m^t\right)}{X_m^c X_m^t} \ , \tag{9}$$

Excerpt from ISBN 978-3-00-053387-7

$$d_m = 1 - \frac{e^{A_m\left(3-\sqrt{7+2r_m^2}\right)}}{\sqrt{7+2r_m^2}-2}, \tag{10}$$

where A_m is a parameter that is computed individually for each element as function of its characteristic length. The fibre-matrix interface is modelled using Abaqus® surface-based cohesive behaviour [7]. Mode dependent cohesive strengths are considered, and the rate of damage progression is controlled by the fracture toughness under mode I, mode II, or mixed-mode, according to the BK law [10].

3. Numerical results

3.1. Results for the AS4 non-hybrid composite

This section is dedicated to the study of the tensile failure of the non-hybrid composite composed of AS4 carbon fibres, whose main properties are: $2R = 7$ mm, $E_1 = 234$ GPa, $\sigma_0 = 4275$ MPa and $m = 10.7$ at $l_0 = 12.7$ mm, the remaining properties can be seen in [2]. To study the effect of the length on both the fibre strength and in the failure mechanisms, RVEs having the same fibre distribution but with different lengths were generated. Another RVE, with a length equal to 15 times the fibre radius, was generated without cohesive surfaces between the fibres and the matrix and, therefore, assuming a perfect bond between these. All these RVEs have dimensions in the direction perpendicular to the fibres equal to 15 times the fibre radius. These results are shown in Figure 2.

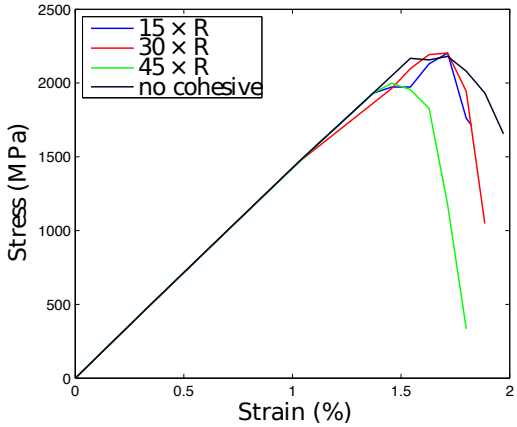

Figure 2. Comparison of the tensile behaviour of AS4 non-hybrid composite for different RVE's.

From the presented results it is observed that the stress-strain curves are very similar for the RVEs with a length of 15 and 30 times the fibre radius. However, the RVE with a length of 45 times the fibre radius failed prematurely, which can be related with random events in the generation of the tensile strength of the elements. The RVE that considers a perfect bond between the fibre and matrix has led to similar results, however, the mechanisms of failure are considered not to be accurately captured in this case.

For the AS4 composite, as the fibres have higher failure strain than the matrix,damage development in the matrix prior to the first fibre failure is observed. This causes some stress concentrations in the fibres in the locations where the matrix is damaged which increases the failure probability in these locations, as represented in Figure 3b. However, analysing the failure locations in multiple simulations, it is observed that the main factor controlling the location of fibre failure is not stress concentrations but the location of the defects, that are simulated as elements with lower failure strength. This is seen not only to dominate first fibre failure but also the subsequent failures. It has been observed that when a fibre fails, the fibre

Excerpt from ISBN 978-3-00-053387-7

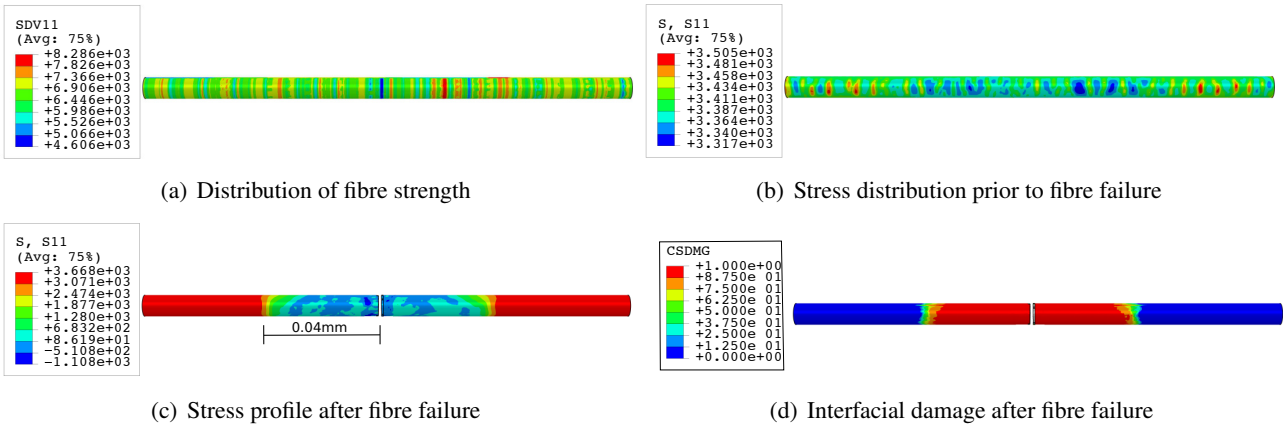

(a) Distribution of fibre strength

(b) Stress distribution prior to fibre failure

(c) Stress profile after fibre failure

(d) Interfacial damage after fibre failure

Figure 3. Failure process in an AS4 carbon fibre.

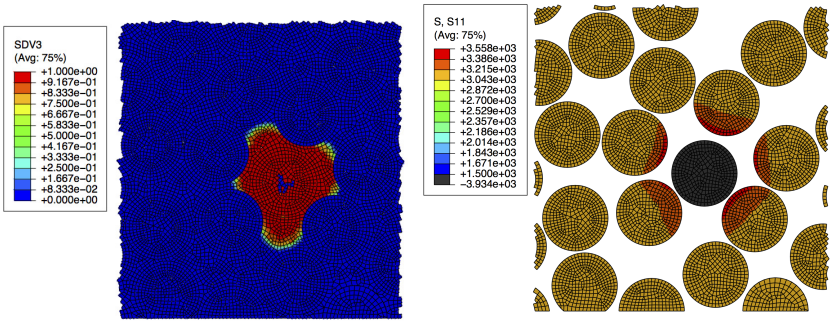

Figure 4. Matrix crack surrounding a broken fibre (on the left) and stress concentrations in intact fibres surrounding a broken one (on the right).

unloads suddenly causing a dynamic effect. The propagation of the stress wave after a fibre break can induce compression stresses in the fibres, which is captured by the model. This makes the fibre lose the load carrying capacity in some of its length, the ineffective length. This effect is captured by the model, as shown in Figure 3. After a fibre breaks a crack in the matrix surrounding this broken fibre can appear, as shown in Figure 4a). The crack progression is hampered by the intact surrounding fibres, that are affected by stress concentrations as shown in Figure 4b). These stress concentrations act in a small region surrounding the broken fibre.The first fibre failure is proceeded by the failure of other fibres. As previously stated, the break location is determined by flaws in the fibres. From the performed analysis it is seen that the majority of the fibres did not fail in the same plane, leading to the formation of a disperse cluster instead of a co-planar one.

3.2. Results for hybrid composites

In this section it is discussed the effects of hybridizing the AS4 carbon composite with M50S carbon fibres [11], whose main properties are:$2R$ = 0.0053 mm, E_1 = 480 GPa, σ_0 = 4600 MPa and m = 9 at l_0 = 10 mm. The results for the hybridization between these two fibres are shown in figure 5, for different RVEs with different volume fractions and considering the fibres to have the same and different radii.

eral RVEs were generated to study this hybridization. The tensile stress-strain curves are shown in Figure 5. All the RVEs studied had dimensions 15 times the radius of the fibre with higher diameter, leading

Excerpt from ISBN 978-3-00-053387-7

to an RVE with a size equal to 52.5 μm. To study the effect of the fibre radius two types of RVEs were generated. The first consider both the AS4 and the M50S carbon fibres to have the same radius, equal to 3.5 μm; the corresponding results are shown in solid lines in Figure 5. The second type of RVEs considered the fibres to have the real fibre radii and, therefore, the AS4 and the M50S were modelled with different radii. The results for these RVEs are shown in Figure 5 in dashed lines. In this figure it is shown the tensile behaviour for hybrid composites with different volume fraction of each fibre type. Those with the same volume fraction of each fibre type are presented with the same colour. Comparing the results for the RVE's with the same radii (solid line) and different radii (dashed line) it is observed that considering of the M50S to be equal to 2.65 μm, higher tensile strength is obtained, for all the hybrid volume fractions analysed. Varying the volume fraction of each fibre type drastically changes the response of the composite material. In all cases, there is no interaction in the failure of both fibre types, this is, all the LE fibres fail prior to the failure of any HE fibres. This causes the first load drop seen for all hybrid composites. However, as we increase the volume content of HE fibres the load drop is reduced, being minimum for a volume fraction of M50S fibres equal to 0.25 (curves in red).

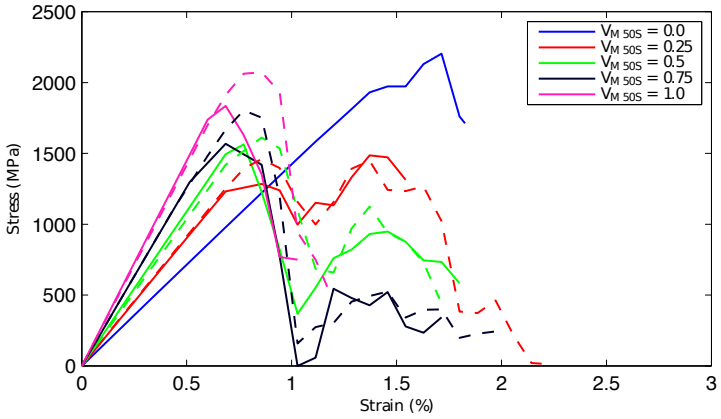

Figure 5. Stress-strain diagrams for AS4-M50S hybrid composites with various hybrid volume fractions: full - RVEs with all fibres with radius equal to 3.5 μm; dashed - RVE's with the M50S with radius equal to 2.65 μm.

The stress-strain curves for the hybrid composite with a volume fraction of M50S fibres equal to 0.25 are again shown in Figure 6a) alongside the microstructure of the RVE, where the circles in full represent broken fibres while the others represent intact fibres. Analysing the microstructures it is possible to note that all the LE fibres (M50S fibres) fail prior to the failure of a single high elongation fibre. This failure causes the first load drop seen in the curves. After the first load drop, as the HE fibres are still intact, the material is still able to carry stress which causes the increase in load after the first drop. At the second load peak, the failure strain of the HE has been reached which causes their failure and the failure of the material. Between both load peaks it is seen that, usually, the LE fibres keep on fracturing leading to the fragmentation of these fibres in multiple locations, which is responsible for the non-linearities seen between the failure of the LE and HE fibres. The tensile response for this hybridization is close to what is described as pseudo-ductility, for a volume fraction of M50S fibres equal to 0.25, however, there is a small load drop after the failure of the LE fibres and prior to the failure of the HE fibres, typical of hybrid composites.

In Figure 6b) it is shown the comparison between the micromechanical model and the global load sharing model proposed by Turon et al. [12] and extended to hybrid composites by Tavares et al. [2]. From the presented results it is possible to conclude that the composite damage model clearly over predicts the results from the micromechanical model. These results are expected as it is seen that the global load sharing models, over predict the experimental results, as what drives the failure are local effects.

Excerpt from ISBN 978-3-00-053387-7

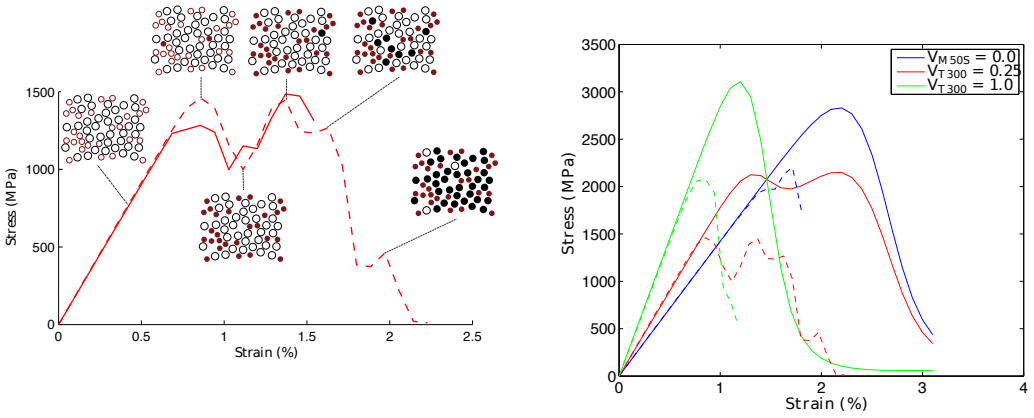

(a) (b)

Figure 6. a)Stress-strain curves and microstructures for the hybrid composite with a volume fraction of M50S carbon fibres equal to 0.25: circles in full represent broken fibres; b) Comparison of the results from the micromechanical model (dashed lines) with the composite damage model (solid lines) for the AS4 and M50S hybridization.

4. Conclusion

A micromechanical model that takes into account the fibre strength variability, and it is able to capture the main failure mechanisms in unidirectional composite materials was developed. From this model it was possible to establish the failure sequence in unidirectional composites, which was seen to be similar to what was previously reported in the literature. For hybrid composites it was possible to determine the complete tensile response of the composite, including the load drop after the failure of the LE fibres and the second load drop due to the failure of the HE fibres. It was concluded that the Weibull modulus plays a critical role in the catastrophic failure of composites. A lower Weibull modulus, higher strength variability, leads to a more gradual failure, that in conjunction with the failure of the HE fibres prior to the complete failure of the LE fibres are the key parameters to achieve pseudo-ductility.

References

[1] Yentl Swolfs, Larissa Gorbatikh, and Ignaas Verpoest. Fibre hybridisation in polymer composites: A review. *Composites Part A: Applied Science and Manufacturing*, 67(0):181 – 200, 2014.

[2] Rodrigo P Tavares, António R Melro, Miguel A Bessa, Albert Turon, Wing K Liu, and Pedro P Camanho. Mechanics of hybrid polymer composites: analytical and computational study. *Computational Mechanics*, pages 1–17, 2016.

[3] A.E. Scott, I. Sinclair, S.M. Spearing, A. Thionnet, and A.R. Bunsell. Damage accumulation in a carbon/epoxy composite: Comparison between a multiscale model and computed tomography experimental results. *Composites Part A: Applied Science and Manufacturing*, 43(9):1514 – 1522, 2012.

[4] M. Ibnabdeljalil and W.A. Curtin. Strength and reliability of fiber-reinforced composites: Localized load-sharing and associated size effects. *International Journal of Solids and Structures*, 34(21):2649 – 2668, 1997.

[5] Yentl Swolfs, Robert M. McMeeking, Ignaas Verpoest, and Larissa Gorbatikh. The effect of fibre dispersion on initial failure strain and cluster development in unidirectional carbon/glass hybrid composites. *Composites Part A: Applied Science and Manufacturing*, 69(0):279 – 287, 2015.

Excerpt from ISBN 978-3-00-053387-7

[6] A.R. Melro, P.P. Camanho, and S.T. Pinho. Generation of random distribution of fibres in long-fibre reinforced composites. *Composites Science and Technology*, 68(9):2092 – 2102, 2008.

[7] Dassault Systemes Simulia. Abaqus 6.12 documentation. *Providence, Rhode Island, US*, 2012.

[8] ZdeněkP. Bažant and B.H. Oh. Crack band theory for fracture of concrete. *Matériaux et Construction*, 16(3):155–177, 1983.

[9] A.R. Melro, P.P. Camanho, F.M. Andrade Pires, and S.T. Pinho. Micromechanical analysis of polymer composites reinforced by unidirectional fibres: Part I - constitutive modelling. *International Journal of Solids and Structures*, 50(11–12):1897 – 1905, 2013.

[10] M.L. Benzeggagh and M. Kenane. Measurement of mixed-mode delamination fracture toughness of unidirectional glass/epoxy composites with mixed-mode bending apparatus. *Composites Science and Technology*, 56(4):439 – 449, 1996.

[11] Fumihiko Tanaka, Tomonaga Okabe, Haruki Okuda, Ian A. Kinloch, and Robert J. Young. Factors controlling the strength of carbon fibres in tension. *Composites Part A: Applied Science and Manufacturing*, 57(0):88 – 94, 2014.

[12] A. Turon, J. Costa, P. Maimí, D. Trias, and J.A. Mayugo. A progressive damage model for unidirectional fibre-reinforced composites based on fibre fragmentation. part I: Formulation. *Composites Science and Technology*, 65(13):2039 – 2048, 2005.

Excerpt from ISBN 978-3-00-053387-7